Electrical control over perpendicular magnetization switching driven by spin-orbit torques

X. Zhang, C. H. Wan,* Z. H. Yuan, Q. T. Zhang, H. Wu, L. Huang, W. J. Kong, C. Fang, U. Khan, and X. F. Han†
Institute of Physics, Chinese Academy of Sciences, Beijing National Laboratory for Condense Matter Physics, Beijing 100190, China
(Received 29 April 2016; revised manuscript received 30 October 2016; published 22 November 2016)

Flexible control of magnetization switching by electrical means is crucial for applications of spin orbitronics. Besides a switching current that is parallel to an applied field, a bias current that is normal to the switching current is introduced to tune the magnitude of effective damping-like and field-like torques and further electrically control magnetization switching. Symmetrical and asymmetrical control over the critical switching current by the bias current with opposite polarities is realized in both Pt/Co/MgO and α-Ta/CoFeB/MgO systems, respectively. This research not only identifies the influences of field-like and damping-like torques on the switching process, it also demonstrates an electrical method to control it.

DOI: 10.1103/PhysRevB.94.174434

I. INTRODUCTION

Spin orbitronics [1,2], aiming at current or voltage control of magnetization (**M**) via the spin-orbit coupling (SOC) effect, is prospective for nonvolatile magnetic storage and programmable spin-logic applications. The spin Hall effect (SHE) in heavy metals [3–6] or topologic insulators [7] and the Rashba effect [8,9] at heavy-metal/ferromagnetic-metal interfaces are two broadly utilized effects to realize spin orbitronics due to their large SOC strength. With the aid of a magnetic field, SHE induced magnetization switching has already been realized in many systems comprising a magnetic layer (Co, CoFeB, NiFe) sandwiched by an oxide layer (AlO_x, MgO) and a heavy-metal layer (Pt, β-Ta, W) not only with in-plane anisotropy [10,11] but with perpendicular anisotropy [12–15]. Recently, field-free magnetization switching via current has also been achieved in wedge-shaped Ta/CoFeB/TaO_x [16] or antiferromagnetic/ferromagnetic coupled perpendicular systems [17–21].

In these perpendicular systems, current can generate via SHE a damping-like torque which balances effective torques from perpendicular anisotropy and in-plane bias field and consequently switches magnetization when it becomes large enough. In these previous researches, mainly spin Hall torque induced by one current (namely, switching current I) applied along the direction of an applied or effective magnetic field is taken into account while the influence of field-like torque on the magnetic reversal process is still lack of systematic research, though some experimental studies have demonstrated its positive role [17,22–24]. Some theoretical work also indicates its effectiveness in reducing critical current, however only with appropriate polarity [25].

Here, we introduce another current (namely, bias current I_B along x axis) to electrically control the magnetization switching process [Fig. 1(a)]. For perpendicularly magnetized systems, the bias-current-induced damping-like (field-like) torque has the same symmetry as the switching-current-induced field-like (damping-like) torque. Therefore, as shown below, the influences of both field-like torque and damping-like torque of the switching current on the magnetization switching process become visible with tuning the magnitude of the bias current. Furthermore, the main features of the aforementioned results can be qualitatively reproduced by a macrospin model which provides further understanding. This work can not only help to distill the influences of different kinds of torques on the switching process but also demonstrate a practical manner of controlling a SHE-driven magnetization switching process by electrically tuning the magnitude of effective damping-like and field-like torques.

II. EXPERIMENTAL METHOD

SiO_2//Ta(5)/$Co_{20}Fe_{60}B_{20}$(1)/MgO(2)/Pt(3) and SiO_2//Pt(5)/Co(0.8)/MgO(2)/Pt(3) (thicknesses in nanometers) stacks were provided by Singulus GmbH. They were magnetron-sputtered at room temperature. They have intrinsically in-plane anisotropy. After annealing at 400 °C and 10^{-3} Pa for 1 h in a perpendicular field of 0.7 T, the stacks exhibited strong perpendicular magnetic anisotropy (PMA). Raw films were then patterned by ultraviolet lithography and subsequet two-step argon ion etching into Hall bars, with the size of the center squares being 20 μm [Fig. 1(a)]. Cu(10 nm)/Au(30 nm) electrodes were finally deposited to make contacts with four legs of the Hall bars. After device microfabrication, the Hall bars were measured with two Keithley 2400 source meters and a Keithley 2182 voltmeter, as sourcing devices and for measuring Hall voltages, respectively. Meanwhile, a physical property measurement system (PPMS-9T, Quantum Design) provided magnetic fields with proper directions. The two Keithley 2400 source meters first provided the current pulses to the Hall bar. One applied switching current along the y axis and the other applied bias current along the x axis to the sample with a duration time of 50 ms. Then the two Keithley 2400 devices were switched off after the duration time. After waiting for 100 ms, one Keithley 2400 device applied another current pulse of 1 mA along the y axis to the sample for 100 ms. At the end of this pulse, the Keithley 2182 meter picked up the Hall voltage along the x axis. Then the Keithley 2400 device was switched off. After 100 ms, the next round of the destabilizing-measuring process was performed.

*wancaihua@iphy.ac.cn
†xfhan@iphy.ac.cn

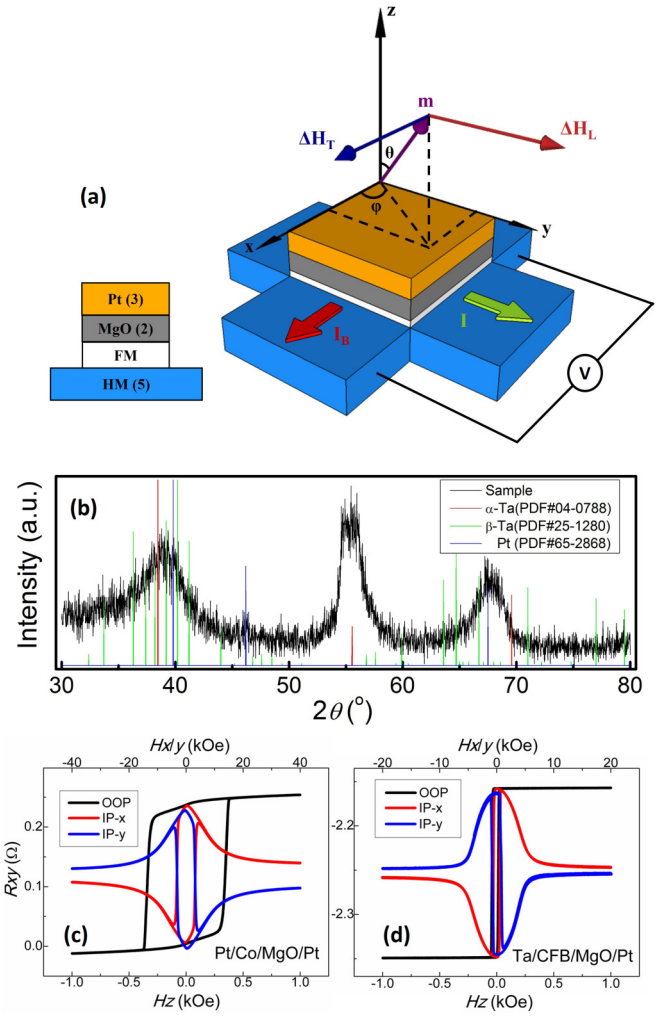

FIG. 1. (a) Sample structure of a Hall bar. ΔH_L and ΔH_T stand for the current-induced effective fields longitudinal and transverse to the current, respectively. (b) Glancing XRD pattern of $Ta/Co_{20}Fe_{60}B_{20}/MgO/Pt$ stacks. (c) and (d) show H dependence of Hall resistance of PCM and TFM, respectively, with fields along the x, y, and z axes. The Hall resistance $R_{xy} \equiv V_x/I_y$ in (c) and (d) is obtained with $I_y = 1$ mA and $I_{Bx} = 0$.

III. RESULTS AND DISCUSSION

A. Experiment

Two typical perpendicular systems, Sub//Pt(5)/Co(0.8)/MgO(2)/Pt(3) (PCM for short) and Sub//Ta(5)/$Co_{20}Fe_{60}B_{20}$(1.0)/MgO(2)/Pt(3) (TFM), are used for comparison. The x-ray diffraction (XRD) characterization of our TFM sample is shown in Fig. 1(b). The strongest peak at 55.8° can only be ascribed to α-Ta (200). The small peak at 46.5° is due to Pt. The other two peaks can be partially attibuted to Pt and α-Ta as indicated by the standard PDF patterns. However, the peak at 39° is wider than the peak at 68°, which indicates formation of some portion of β-Ta in the α-Ta matrix. Meanwhile, we also conducted four-probe resistivity measurements to further check the phase of the Ta film. The resistivity of Ta in our sample is 8.8×10^{-7} Ω m which is closer to that of α-Ta. The resistivity for α-Ta is less than 1.0×10^{-6} Ω m, while ρ_{xx} is 1.8–2.2 $\times 10^{-6}$ Ω m for β-Ta [26,27]. Thus XRD and resistivity data both indicate that the α-Ta phase occupies half or even more content in our stacks.

M_0t of PCM and TFM measured by vibration sample magnetometry is 125 μemu/cm^2 and 145 μemu/cm^2, respectively. M_0 and t are saturated magnetization and thickness of magnetic layer, respectively. Hall measurement demonstrates PMA of both systems. It has been observed that PCM shows higher PMA energy than TFM. The anisotropy field (H_{an}) of PCM and TFM is about 13.6 kOe and 5.8 kOe, respectively [Figs. 1(c) and 1(d)]. A sophisticated harmonic lock-in technique [28,29] is applied here to characterize spin-orbit effective fields ($\Delta H_{L/T}$) of the above systems induced by applied current. The effective longitudinal field ΔH_L and effective transverse field ΔH_T corresponding to damping-like torque and field-like torque, respectively, are shown in Fig. 1. The definition of coordinates and sample structure are also shown [Fig. 1(a)].

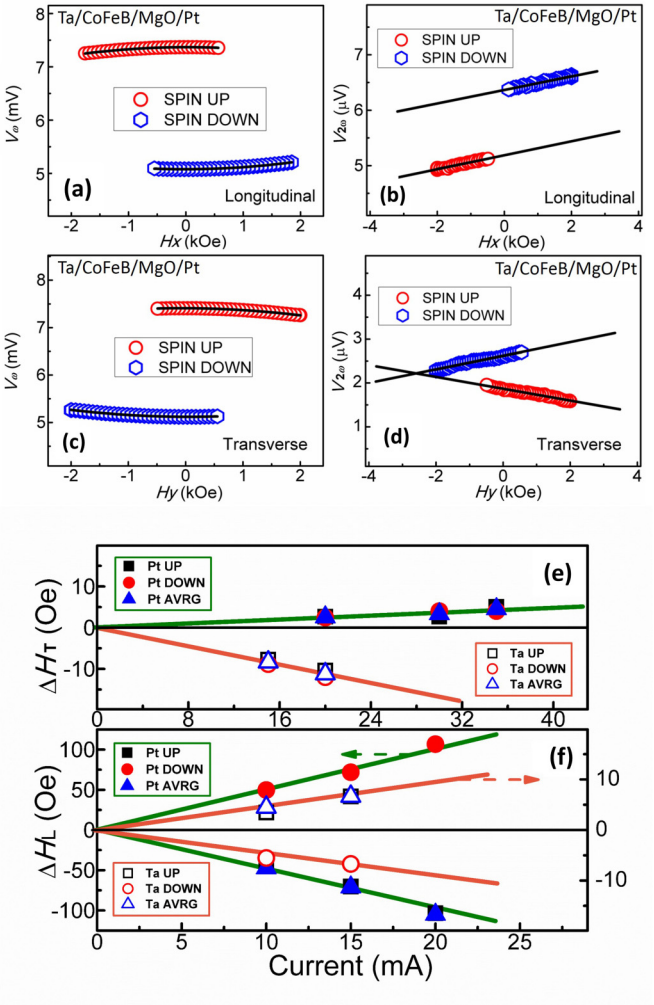

FIG. 2. The H_y dependence of (a) V^{ω} and (b) $V^{2\omega}$ and the H_x dependence of (c) V^{ω} and (d) $V^{2\omega}$ in TFM. (e) and (f) show, respectively, the current dependence of ΔH_T and ΔH_L in both TFM and PCM films. Their linear fittings with zero intercept are also shown. When measuring the effective fields induced by the switching current, we applied no bias current. FM and HM denote ferromagnetic and heavy metal, respectively.

During measurement, current density ($j_y = j_{y0}\sin\omega t$) is applied along the $+y$ axis. The magnetic field (H) is applied along the x or y axis. The direction of H determines which torque can be detected. H_x and H_y are respectively used to measure current-induced effective transverse field ΔH_T and effective longitudinal field ΔH_L. The effective fields ΔH_L and ΔH_T correspond to damping-like torque and field-like torque, respectively. First and second harmonic Hall voltages along the x axis ($V_x^\omega = V_{x0}^\omega \sin\omega t$ and $V_x^{2\omega} = V_{x0}^{2\omega}\cos 2\omega t$) are picked up to indirectly show direction of magnetization ($\mathbf{M}$) with respect to the $+z$ axis and j_y-tuned $\mathbf{M}$ change, accordingly. V_{x0}^ω and $V_{x0}^{2\omega}$ exhibit parabolic and linear field dependence for $\mathbf{M}$ around $\pm z$, respectively. Especially, the $V_0^{2\omega}$ vs H curves [Fig. 2(b)] exhibit the same slopes at $\pm m_z$ when H is along y, while they exhibit opposite slopes when H is along x [Fig. 2(d)]. From the slopes as well as $\partial^2 V^\omega/\partial H^2$ [Figs. 2(a) and 2(c)] we can obtain ΔH_L along the y axis and ΔH_T along the x axis via $\Delta H_{L/T} = -2(\partial V^{2\omega}/\partial H_{y/x})/(\partial^2 V^\omega/\partial H_{y/x}^2)$. Here $\Delta\mathbf{H}_L$ parallel to $\boldsymbol{\sigma}\times\mathbf{M}$ originates from the spin Hall effect. $\Delta\mathbf{H}_T$ parallel to $\boldsymbol{\sigma}$ originates from the Rashba field as well as the Oersted field. $\boldsymbol{\sigma}$ is the spin current density induced by $\mathbf{j}_y$ via $\boldsymbol{\sigma}\propto\mathbf{j}_y\times\mathbf{z}$. Besides, an appreciable planar Hall effect would lead to corrections to the expression of the effective field [30]. However, in contrast to the remarkable planar Hall effect in Ref. [20,31], no observable planar Hall effect signal was detected in the Hall measurement with an in-plane magnetic field for both systems [Figs. 1(c) and 1(d)]. Moreover, the planar Hall resistance of both systems was evaluated to be less than 0.01 Ω by anisotropic magnetoresistance measurements, which is negligible compared to the anomalous Hall resistance of 0.2 Ω.

$\Delta H_{L/T}$ shows linear dependence on applied current density j_y with zero intercepts as expected. Parameter $\beta_{L/T}$, defined as $d\Delta H_{L/T}/dj_y$, characterizes the conversion efficiency from charge current to effective field. Here, $j_y = I/(wh_{HM})$. I is the switching current, w is the width of the Hall bar (20 μm) and h_{HM} is the thickness of the heavy metal (5 nm). 1 mA of I thus corresponds to 1 MA/cm^2 of j_y. The shunting effect of the ferromagnetic layer and antioxidation layer is ignored. Thus, j_y and $\beta_{L/T}$ should be deemed upper and lower bounds, respectively. β_L is about -5 Oe/(MA/cm^2) and $+0.5$ Oe/(MA/cm^2) for PCM and TFM, respectively [Fig. 2(e)]. Meanwhile, the β_T is about $+0.15$ Oe/(MA/cm^2) and -0.5 Oe/(MA/cm^2) for PCM and TFM, respectively [Fig. 2(f)]. Especially, $\beta_{L/T}$ of Ta and Pt have opposite signs. $\beta_{L/T}$ of Pt is reported in the range of 0.1–10 Oe/(MA/cm^2) [9,10,13,28,32] in different systems. Our value is closer to that of Liu [13] and Fan [10]. Besides, $|\beta_{L,Pt}| \gg |\beta_{T,Pt}|$, consistent with the results of Liu [13]. The $\beta_{L/T}$ of Ta in the Ta/CoFeB/MgO system was thoroughly researched by Kim [29]. It is in the range of 0.1–4 Oe/(MA/cm^2), depending on thickness of Ta and CoFeB. Besides, their results show $\beta_{T,Ta}$ can be comparable to and even larger than $\beta_{L,Ta}$. Our measured values are within their range and $|\beta_{L,Ta}|$ is equal to $|\beta_{T,Ta}|$. However, the β_L of Ta here is smaller than that of β-Ta [29], probably due to larger content of α-Ta in our sample. The ratio of β_T/β_L for Pt and Ta is -0.03 and -1, respectively. Field-like torque can be nearly neglected in PCM while it cannot be ignored in TFM, which provides us a couple of ideal systems to research the influence of field-like torque and damping-like torque on switching behavior of perpendicular films. The reason why field-like torque is insignificant and significant in PCM and TFM respectively, we think, is that the two systems may have different interfacial potentials due to different work functions of Pt (5.3 eV), Co (4.4 eV), Fe (4.3 eV), and Ta (4.1 eV) [33,34] as elaborated in Ref. [35].

In the following, we will use PCM with $\beta_T/\beta_L = -0.03$ and TFM with $\beta_T/\beta_L = -1$ to study the influence of I_B on switching behaviors and introduce the underlying mechanism based on a macrospin model. I and H_y are applied along y. I_B is applied along x. As $I_B = 0$, $\mathbf{M}$ can be switched back and forth between spin-up state and spin-down state (Fig. 3) by scanning I under nonzero H_y. Due to opposite spin Hall angles, the switching direction is opposite for PCM and TFM with the same measurement setup. For example, the switching direction for TFM and PCM is clockwise and anticlockwise, respectively, at positive H_y. Sign reversal of H_y leads to reversal of the switching direction. Figure 3 also shows that nearly a full magnetization switching can be realized when $H_y = 0.3$ kOe for TFM. In this condition, the critical switching current (I_C) is 63.5 mA. Here, I_C is defined as the current corresponding to $(R_+ + R_-)/2$ where R_+ and R_- are the saturation resistances of positive current and negative current, respectively. Meanwhile, the I_C for PCM is about 80 mA when $H_y = 0.7$ kOe. These results manifest that Ta containing a substantial α phase can also function as a high

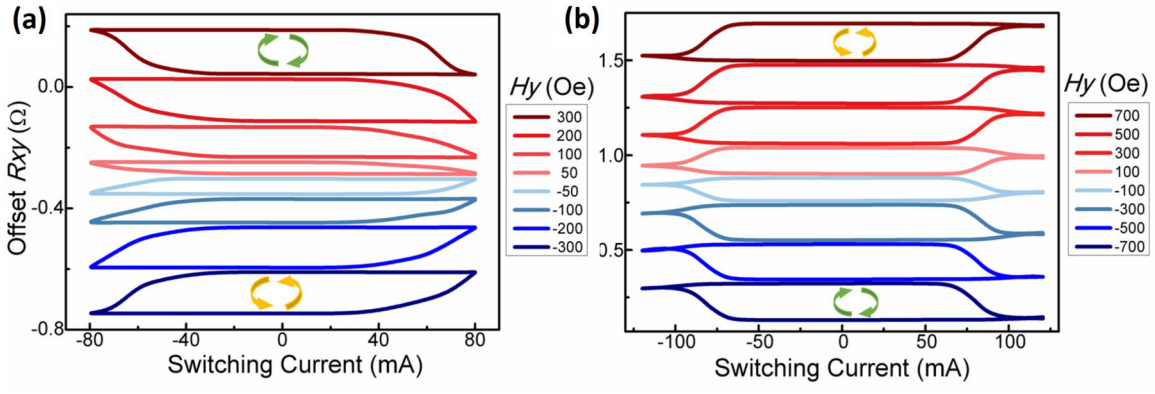

FIG. 3. The dependence of R_{xy} on switching current (I) in (a) TFM and (b) PCM systems under different H_y.

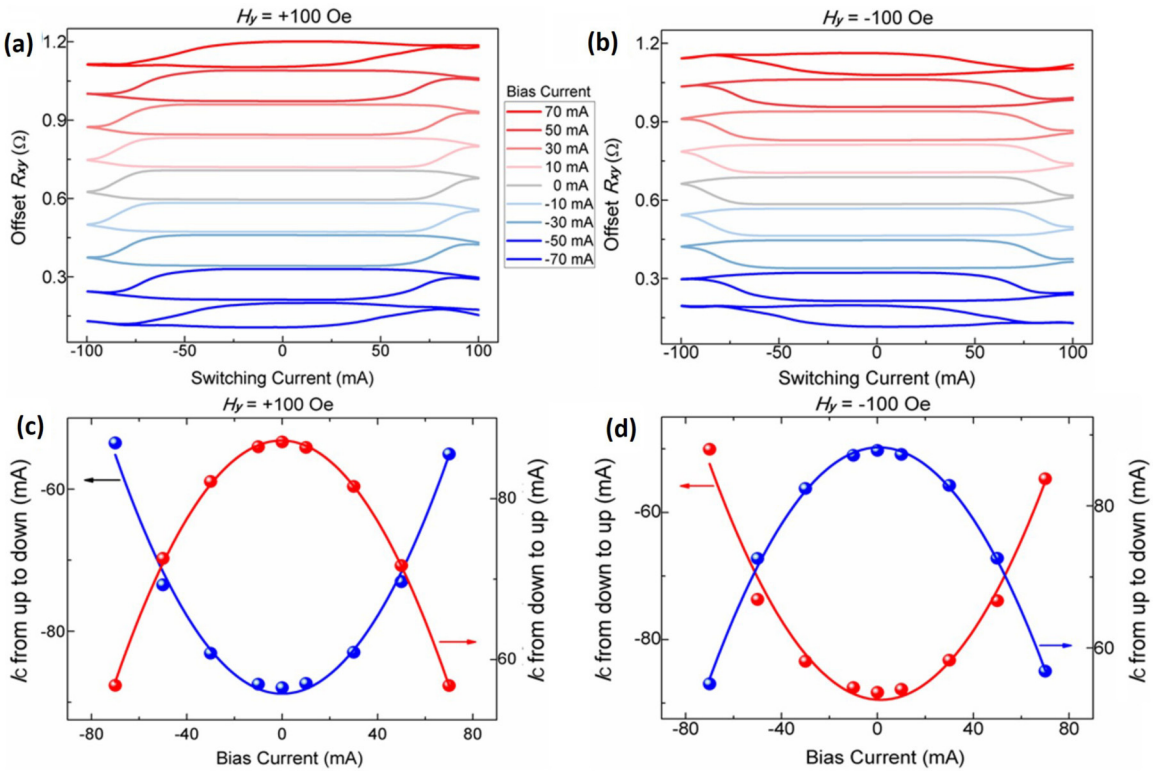

FIG. 4. The switching current dependence of R_{xy} of PCM under different bias currents with (a) $H_y = 100$ Oe and (b) -100 Oe and the dependence of I_C on I_B with (c) $H_y = 100$ Oe and (d) -100 Oe. Red and blue dots in (c) and (d) show, respectively, the I_C of transitions from down state to up state and from up state to down state. The dependence of I_C on I_B in (c) and (d) could be well reproduced by parabolic fittings.

efficiency converter from charge current to spin current besides of Pt and β-Ta.

As shown in Figs. 4(a) and 4(b), elevated I_B can significantly reduce the I_C in the PCM system. For example, $I_C = 88$ mA when $I_B = 0$ mA while $I_C = 73$ mA when $I_B = 50$ mA. I_C decreases by 17%. Meanwhile, positive and negative I_B leads to nearly the same amount of reduction, no matter the sign of H_y, as shown by the parabolic fitting lines in Figs. 4(c) and 4(d). This I_B-induced decrease in I_C can be ascribed to the damping-like torque from I_B as shown in the theoretical part below. It is worth emphasizing that the damping-like torque of I_B shares a similar symmetry with the field-like torque of I, and thus a large field-like torque of I could also in principle reduce the I_C.

Certainly, I_B will heat magnetic films as well and in principle reduce the effective H_{an}, which could also reduce I_C. In order to rule out the possibility of Joule heating, a Pt(5)/Co(0.8)/Pt(5) (PCP) stack possessing coercivity and saturation fields comparable with the PCM stacks was fabricated for comparison. In this control sample, net damping-like and field-like spin-orbit torques are both absent, and therefore the Joule heating becomes the only possible factor of current-induced coercivity reduction. In this regard, we measured the R_{xy} vs H curves at elevated currents of both systems. The switching field in the PCM system decreases remarkably with increasing measuring current, while it remains very stable regardless of the current in the PCP system (not shown here). This contrast indicates the dominance of SOT in the process of magnetization switching in our PCM sample.

On the other hand, the TFM system manifests a different response to I_B with different symmetry in comparison with the PCM counterpart. As shown in Figs. 5(a) and 5(c) for $H_y = +100$ Oe and the transition from down state to up state, I_C is reduced by about 67% under $I_B = 40$ mA while it is only reduced by 20% under $I_B = -40$ mA. In contrast, for $H_y = -100$ Oe and the transition from up state to down state [Figs. 5(b) and 5(d)], besides the opposite switching direction, the effect of I_B on I_C is al so reversed; i.e., I_C decreased only by about 5% under $I_B = 40$ mA while it decreased remarkably by 53% under $I_B = -40$ mA. Here, the asymmetric response of I_C to positive and negative I_B cannot be interpreted by damping-like torque induced by I_B or heating effect as shown in the case of PCM. Instead, field-like torque of I_B is a key contributor to the asymmetry as shown below.

B. Macrospin model

In order to interpret the different responses of PCM and TFM to I_B, we have turned to a macrospin model (more details are in the Appendix). The magnetic energy includes uniaxial anisotropy energy $K \sin 2\theta$ and Zeeman energy $-H_y M_0 \sin\theta \sin\varphi$, where θ and φ are the polar angle between $\mathbf{M}$ and the $+z$ axis and the azimuthal angle between in-plane projection of $\mathbf{M}$ and the $+x$ axis, respectively [Fig. 1(a)]. I and I_B provide both a damping-like torque and a field-like torque on $\mathbf{M}$ with efficiency characterized by β_T/β_L. We use parameter a in units of $H_{an} \equiv 2K/M_0$ to denote the

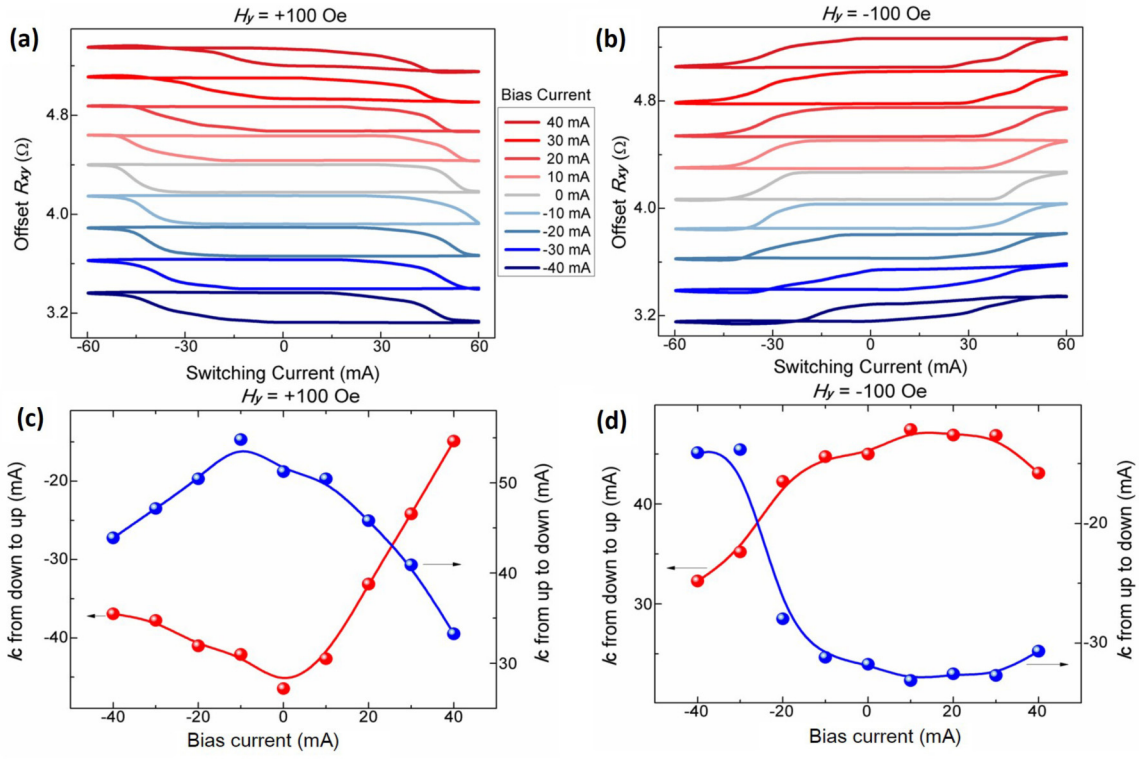

FIG. 5. The switching current dependence of R_{xy} of TFM under different bias currents with (a) $H_y = +100$ Oe and (b) -100 Oe and the dependence of I_C on I_B with (c) $H_y = +100$ Oe and (d) -100 Oe.

damping-like torque provided by I, parameter c to denote the ratio of I_B/I, and parameter b to denote the ratio β_T/β_L. Actually, c reflects the angle of total current density with respect to the direction of magnetic field. As I and I_B are both applied, the torque equilibrium condition requires satisfaction of Eq. (1):

$$0 = \vec{m} \times \vec{H}_{\text{eff}} + a\vec{m} \times (-\hat{e}_x) \times \vec{m} + ab\vec{m} \times (-\hat{e}_x) + ac\vec{m} \times \hat{e}_y \times \vec{m} + abc\vec{m} \times \hat{e}_y. \quad (1)$$

Here $\mathbf{H}_{\text{eff}} = -\nabla_M E$, $\mathbf{m} \equiv \mathbf{M}/M_0$, $E \equiv K \sin^2\theta - M_0 H_y \sin\theta \cos\varphi$, e_x and e_y are unit vectors along the x and y axes, respectively. The second and third terms in the right-hand side of Eq. (1) are damping-like and field-like torques from I while the fourth and fifth terms are damping-like and field-like torques from I_B, respectively. Equation (1) can be further reduced to scalar equations. Equation (2) is one of them:

$$\sin\theta\cos\theta - \frac{\left[a^2(b^2+1)(c^2+1) + h_y^2 - 2abch_y\right]}{h_y - a\cos\theta - abc} \times \cos\theta \sin\varphi + \frac{ah_y(1+\cos^2\theta)}{h_y - a\cos\theta - abc}\sin\varphi = 0. \quad (2)$$

If $I_B = 0$ and $b = 0$, $\sin\theta\cos\theta - h_y\cos\theta\sin\varphi + a\sin\varphi = 0$, which shares a form similar to that derived by Liu [13] and Yan [36]. Here $h_y \equiv H_y/H_{\text{an}}$. Comparing Eq. (2) with the simplified one for $I_B = 0$ and $b = 0$, we can see that the introduction of I_B leads to an effective h_y^{eff} and an effective damping-like torque a^{eff} as expressed in Eq. (3):

$$h_y^{\text{eff}} = \frac{\left[a^2(b^2+1)(c^2+1) + h_y^2 - 2abch_y\right]}{h_y - a\cos\theta - abc}, \quad (3a)$$

$$a^{\text{eff}} = \frac{ah_y(1+\cos^2\theta)}{h_y - a\cos\theta - abc}. \quad (3b)$$

Simulated results according to Eq. (1) are shown in Fig. 6 where $\tau_C \propto I_C$ is the critical damping-like torque of I. As $c = 0$, a nonzero b can significantly reduce the critical switching current (I_C), regardless of its sign [Fig. 6(g)]. I_C decreases by 5.8% and 42% for $b = \pm 1$ and $b = \pm 3.6$ [29], respectively, compared with I_C for $b = 0$. This trend is consistent with the result in the PCM sample in which the damping-like torque of I_B can mimic the influence of the field-like torque of I. Though it cannot reverse $\mathbf{M}$ directly, a large Rashba effect can still help to effectively reduce I_C.

As $b = 0$, bias current ($c \neq 0$) can notably decrease I_C and the amount of the reduction in I_C does not depend on the polarity of c [Figs. 6(a) and 6(b)], which manifests characteristics similar to those of the switching behaviors of the PCM sample. For $b = -1$ and $h_y = 0.4$ [Fig. 6(c)], $c = 0.3$ and $c = -0.3$ will result in asymmetric decrease in I_C. Here $c = -0.3$ is more effective in reducing I_C. However, for $h_y = -0.4$ [Fig. 6(d)], I_C decreases more in the case of $c = +0.3$. These characteristics [Figs. 6(c) and 6(d)] qualitatively reproduce the results of the TFM sample in Figs. 5(a) and 5(b). Figures 6(e) and 6(f) show the I_B dependence of I_C as $b = 0$ and $b = -1$, respectively. The former indeed predicts

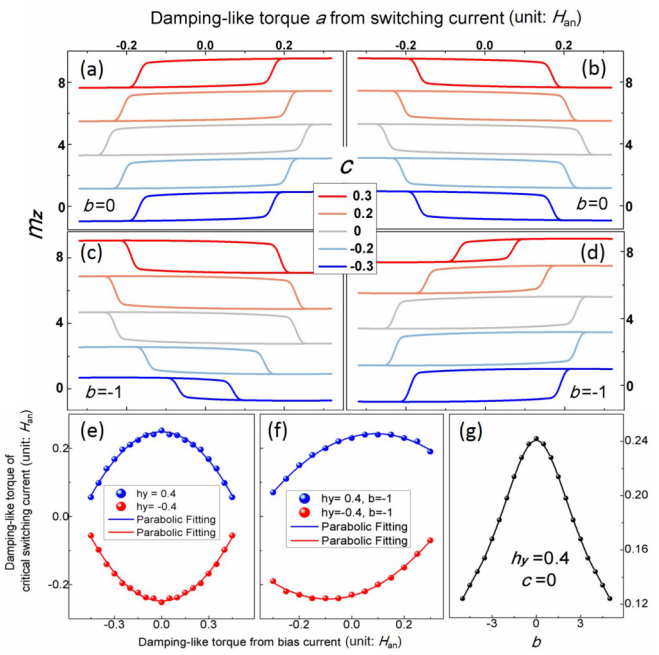

FIG. 6. Dependence of m_z on damping-like torque of switching current a (in units of H_{an}) for different c, for (a) $h_y = 0.4$, (b) $h_y = -0.4$ with $b = 0$, (c) $h_y = 0.4$, and (d) $h_y = -0.4$ with $b = -1$. (e) and (f) τ_c as a function of damping-like torque of I_B under $h_y = \pm 0.4$ for $b = 0$ and $b = -1$, respectively. Here τ_c is obtained by the transition from spin-down to spin-up state. (g) τ_c as a function of b for $c = 0$ and $h_y = 0.4$.

a parabolic dependence as observed in Figs. 4(c) and 4(d) while the latter also predicts a linear dependence besides the parabolic one, which qualitatively reproduces the results in Figs. 5(c) and 5(d). It is worth noting that field-like torque and damping-like torque are both indispensable to realize the asymmetry reduction of I_C under opposite I_B. Figure 5 also indirectly manifests that the two types of torque both play important roles in the magnetization switching process of the TFM system.

Other Pt/Co/MgO and Ta/CoFeB/MgO samples have exhibited similar switching symmetries. Notably, though we demonstrate the switching behaviors with aid of an applied field, the switching performance controlled by I_B will be still achievable in principle if the applied field is replaced by an effective field from exchange coupling.

Recent studies on domain wall motion induced magnetization switching points out that a large in-plane field H_y will make the domain walls become Néel type, the center spin of which is in the direction of H_y [22,37–39]. When a current $\mathbf{J}_{\text{write}}$ parallel to the H_y is applied, a spin current $\boldsymbol{\sigma}$ polarized in the x direction is absorbed by the center spins $\mathbf{m}_{\text{DW}}$ of the domain wall, which exerts an effective field $\boldsymbol{H}_z^{\text{eff}} = \boldsymbol{\sigma} \times \mathbf{m}_{\text{DW}}$ to the domain wall. The H_z^{eff} is along the z direction, resulting in domain wall motion [40]. The above discussion is based on the condition of no $\mathbf{J}_{\text{bias}}$. Let us consider a system with negligible field-like torque such as PCM. If $\mathbf{J}_{\text{bias}}$ is turned on, polarization of the spin current σ' generated by $\mathbf{J}_{\text{bias}}$ is then in the y axis. In this case, $H_{\text{bias}}^{\text{eff}} = \boldsymbol{\sigma}' \times \mathbf{m}_{\text{DW}} = 0$ since $\boldsymbol{\sigma}'$ is parallel (or antiparallel) to $\mathbf{m}_{\text{DW}}$, indicating that the bias current might not play a significant role in domain wall motions or switching behaviors in this toy model. Thus the aforementioned model in this way may not explain our observations.

Though the macrospin model adopted in this work qualitatively interprets main features of our results, it is still primitive. The real switching process is likely induced by the nucleation and domain wall motion. Therefore, a more quantitative and precise discussion based on the microspin simulation of our results deserves further investigation in the future.

IV. SUMMARY

Current-induced effective fields of Pt and Ta have been characterized by a second-harmonic technique as $\beta_{\text{L,Pt}} = -5$ Oe/(MA/cm^2), $\beta_{\text{L,Ta}} = +0.5$ Oe/(MA/cm^2), $\beta_{\text{T,Pt}} = +0.15$ Oe/(MA/cm^2) and $\beta_{\text{T,Ta}} = -0.5$ Oe/(MA/cm^2). Current can generate much larger field-like torque in Ta than in Pt. Current-induced magnetization switching has also been realized in the Ta rich α phase, indicating its high enough spin-orbit coupling strength and shedding light on its potential use in spin orbitronics. Field-like torque, though incapable of switching $\mathbf{M}$ directly in our case, plays a crucial role in reducing I_C.

I_B results in different influences on switching behaviors for the TFM and PCM systems. Opposite I_B equally decreases I_C in PCM while it asymmetrically influences I_C in the TFM system. Furthermore this asymmetry originates from the field-like torque of I_B and can be adjusted by the polarity of H_y. Our work not only brings to light the influence of damping-like and field-like torques of switching current and bias current on switching but also experimentally demonstrates an electrical means (via bias current) to symmetrically or asymmetrically control the switching, which could advance the development of spin-logic applications in which control of the switching process via electrical methods is crucial and beneficial.

ACKNOWLEDGMENTS

This work was supported by the 863 Plan Project of Ministry of Science and Technology (MOST) (Grant No. 2014AA032904), the MOST National Key Scientific Instrument and Equipment Development Projects (Grant No. 2011YQ120053), the National Natural Science Foundation of China (NSFC) (Grants No. 11434014, No. 51229101, and No. 11404382) and the Strategic Priority Research Program (B) of the Chinese Academy of Sciences (CAS) (Grant No. XDB07030200).

APPENDIX : DETAILS OF THE MACROSPIN MODEL

The schematic structure of Pt/Co/MgO or Ta/CoFeB/MgO is shown in Fig. 1(a). An applied field H_y and the switching current (I) are along the $+y$ axis. The bias current (I_B) is along the $+x$ axis. The ratio of I_B/I is defined as a parameter c which actually reflects the angle between the direction of total current density and that of the applied field. The easy axis of the perpendicular systems (PCM or TFM) is along the z axis. Therefore the total energy (E)

is $K\sin^2\theta - M_0 H_y \sin\theta\sin\varphi$ with K anisotropy energy and M_0 saturation magnetization. This energy drives an effective field $\mathbf{H}_{\rm eff} = -\nabla_{\rm M} E$. Here we use a macrospin model for simplicity and therefore only θ and φ are variable, with M_0 being a constant. $H_{\theta,\rm eff} = -H_{\rm an}\sin\theta\cos\theta + H_y\cos\theta\sin\varphi$ and $H_{\varphi,\rm eff} = H_y\cos\varphi$; $H_{\rm an} \equiv 2K/M_0$. $H_{\theta,\rm eff}$ and $H_{\varphi,\rm eff}$ are two orthogonal components of $\mathbf{H}_{\rm eff}$. As the currents I and $I_{\rm B}$ are both applied, the magnetization direction will be modulated due to the damping-like and field-like torques originating from I and $I_{\rm B}$. The damping-like torque of a unit of $\mathbf{M}$ induced by I via the spin Hall effect is defined as a parameter a which is proportional to the spin Hall angle and is along the x axis. Then the damping-like torque induced by $I_{\rm B}$ is ac, which is, however, along the y axis. As shown in the main text, $\beta_{\rm L(T)}$ is defined as the effective field corresponding to the damping-like (field-like) torque induced by unit of I. Here we further define b as $\beta_{\rm T}/\beta_{\rm L}$. Thus the field-like torque induced by I via the Rashba effect as well as the Oersted mechanism is ab and is along the y axis. In contrast, the field-like torque induced by $I_{\rm B}$ is abc and is along the x axis. For perpendicularly magnetized systems, it is very important that the direction of the field-like torque induced by I is the same as that of the damping-like torque induced by $I_{\rm B}$. The final state of the system is determined by the following LLG equation (A1):

$$-\frac{1}{\gamma}\frac{d\vec{M}}{M_0 dt} = -\alpha\vec{M}\times\frac{d\vec{M}}{M_0 dt} + \frac{\vec{M}}{M_0}\times\vec{H}_{\rm eff} + a\frac{\vec{M}}{M_0}\times(-\hat{e}_x)\times\frac{\vec{M}}{M_0} + ab\frac{\vec{M}}{M_0}\times(-\hat{e}_x) + ac\frac{\vec{M}}{M_0}\times\hat{e}_y\times\frac{\vec{M}}{M_0} + abc\frac{\vec{M}}{M_0}\times\hat{e}_y. \quad \text{(A1)}$$

In the first line of Eq. (A1), γ and α are the gyromagnetic ratio and damping constant, respectively. The quantities e_x and e_y are unit vectors along the x and y axes, respectively. The first and second terms in the second line are damping-like and field-like torques induced by the switching current (I), respectively. The first and second terms in the third line are damping-like and field-like torques induced by the bias current ($I_{\rm B}$), respectively. At steady state, $d\mathbf{M}/M_0 dt = 0$. Thus we arrive at Eq. (A2):

$$0 = \vec{m}\times\vec{H}_{\rm eff} + a\vec{m}\times(-\hat{e}_x)\times\vec{m} + ab\vec{m}\times(-\hat{e}_x) + ac\vec{m}\times\hat{e}_y\times\vec{m} + abc\vec{m}\times\hat{e}_y \quad \text{(A2)}$$

Here we have replaced $\mathbf{M}/M_0$ with $\mathbf{m}$. Equation (A2) gives the scalar equations (A3), which are also shown in the main text:

$$H_y\cos\varphi - a\cos\theta\cos\varphi - ab\sin\varphi + ac\cos\theta\sin\varphi - abc\cos\varphi = 0, \quad \text{(A3a)}$$

$$H_y\cos\theta\sin^2\varphi - H_{an}\sin\theta\cos\theta\sin\varphi - a\sin^2\varphi + ab\cos\theta\sin\varphi\cos\varphi - ac\sin\varphi\cos\varphi - abc\cos\theta\sin^2\varphi = 0. \quad \text{(A3b)}$$

As $c = b = 0$, Eq. (A3) is reduced to Eq. (A4):

$$(H_y - a\cos\theta)\cos\varphi = 0, \quad \text{(A4a)}$$

$$\sin\varphi(H_y\cos\theta\sin\varphi - H_{an}\sin\theta\cos\theta - a\sin\varphi) = 0. \quad \text{(A4b)}$$

One possible solution as well as the final physically meaningful solution of Eq. (A4) is further reduced to Eq. (A5):

$$\cos\varphi = 0, \quad \text{(A5a)}$$

$$H_{an}\sin\theta\cos\theta - H_y\cos\theta\sin\varphi + a\sin\varphi = 0. \quad \text{(A5b)}$$

This solution shares a form similar to that derived in Refs. [13] and [41], and the critical current density is

$$\sigma_C = \frac{H_{an}}{2} - \frac{H_x}{\sqrt{2}}, \quad \text{(A6)}$$

the same as in Ref. [41], which demonstrates the rationality of our derivations.

In the general case, Eq. (A3) can be transformed as Eq. (A7):

$$\cos\varphi = \frac{(ab - ac\cos\theta)\sin\varphi}{H_y - a\cos\theta - abc}, \quad \text{(A7a)}$$

$$H_{an}\sin\theta\cos\theta - \frac{[(H_y - abc)^2 + a^2(b^2 + c^2 + 1)]}{H_y - a\cos\theta - abc} \times \cos\theta\sin\varphi + \frac{aH_y(1+\cos^2\theta)}{H_y - a\cos\theta - abc}\sin\varphi = 0. \quad \text{(A7b)}$$

Comparing Eqs. (A5b) and (A7b), we find that the introduction of $I_{\rm B}$ actually updates H_y with an effective field of $[(H_y - abc)^2 + a^2(b^2 + c^2 + 1)]/(H_y - a\cos\theta - abc)$ and updates a with an effective torque of $aH_y(1+\cos^2\theta)/(H_y - a\cos\theta - abc)$.

As $c = 0$, the effective field becomes $[H_y^2 + a^2(b^2 + 1)]/(H_y - a\cos\theta)$. A nonzero b can make the effective field larger, which is very beneficial for higher efficient switching. As $b = 0$, the effective field becomes $[H_y^2 + a^2(c^2 + 1)]/(H_y - a\cos\theta)$. Therefore, the introduction of the bias current (or nonzero c regardless of its polarity) can also increase the effective field. Besides, the field-like torque of the switching current (ab) in the former case functions in a role similar to the damping-like torque of the bias current (ac) in the latter case. Only for $b \neq 0$ can c with opposite sign asymmetrically influence the effective field. It is also worth noting that H_y is still indispensable for magnetization switching because a zero H_y will also lead to a zero effective torque. The numerical results regarding the solutions of Eq. (A3) are shown in Fig. 6 in the main text.

[1] T. Kuschel and G. Reiss, Nat. Nanotechnol. **10**, 22 (2014).
[2] A. Manchon, Nat. Phys. **10**, 340 (2014).
[3] M. I. D'Yakonov and V. I. Perel', ZhETF Pis. Red. **13**, 657 (1971) [JETP Lett. **13**, 467 (1971)].

[4] J. E. Hirsch, Phys. Rev. Lett. **83**, 1834 (1999).
[5] S. Zhang, Phys. Rev. Lett. **85**, 393 (2000).
[6] J. Sinova, S. O. Valenzuela, J. Wunderlich, C. H. Back, and T. Jungwirth, Rev. Mod. Phys. **87**, 1213 (2015).
[7] Y. Fan, P. Upadhyaya, X. Kou, M. Lang, S. Takei, Z. Wang, J. Tang, L. He, L.-T. Chang, M. Montazeri, G. Yu, W. Jiang, T. Nie, R. N. Schwartz, Y. Tserkovnyak, and K. L. Wang, Nat. Mater. **13**, 699 (2014).
[8] Y. A. Bychkov and E. I. Rashba, Pis'ma Zh. Eksp. Teor. Fiz. **39**, 66 (1984) [JETP Lett. **39**, 78 (1984)].
[9] I. M. Miron, G. Gaudin, S. Auffret, B. Rodmacq, A. Schuhl, S. Pizzini, J. Vogel, and P. Gambardella, Nat. Mater. **9**, 230 (2010).
[10] X. Fan, J. Wu, Y. Chen, M. J. Jerry, H. Zhang, and J. Q. Xiao, Nat. Commun. **4**, 1799 (2013).
[11] L. Liu, C.-F. Pai, Y. Li, H. W. Tseng, D. C. Ralph, and R. A. Buhrman, Science **336**, 555 (2012).
[12] I. M. Miron, K. Garello, G. Gaudin, P.-J. Zermatten, M. V. Costache, S. Auffret, S. Bandiera, B. Rodmacq, A. Schuhl, and P. Gambardella, Nature (London) **476**, 189 (2011).
[13] L. Liu, O. J. Lee, T. J. Gudmundsen, D. C. Ralph, and R. A. Buhrman, Phys. Rev. Lett. **109**, 096602 (2012).
[14] C.-F. Pai, L. Liu, Y. Li, H. W. Tseng, D. C. Ralph, and R. A. Buhrman, Appl. Phys. Lett. **101**, 122404 (2012).
[15] X. Qiu, K. Narayanapillai, Y. Wu, P. Deorani, D.-H. Yang, W.-S. Noh, J.-H. Park, K.-J. Lee, H.-W. Lee, and H. Yang, Nat. Nanotechnol. **10**, 333 (2015).
[16] G. Yu, P. Upadhyaya, Y. Fan, J. G. Alzate, W. Jiang, K. L. Wong, S. Takei, S. A. Bender, L.-T. Chang, Y. Jiang, M. Lang, J. Tang, Y. Wang, Y. Tserkovnyak, P. K. Amiri, and K. L. Wang, Nat. Nanotechnol. **9**, 548 (2014).
[17] S. Fukami, C. Zhang, S. DuttaGupta, A. Kurenkov, and H. Ohno, Nat. Mater. **15**, 535 (2016).
[18] A. van den Brink, G. Vermijs, A. Solignac, J. Koo, J. T. Kohlhepp, H. J. M. Swagten, and B. Koopmans, Nat. Commun. **7**, 10854 (2016).
[19] Y.-C. Lau, D. Betto, K. Rode, J. M. D. Coey, and P. Stamenov, Nature Nanotech. **11**, 758 (2016).
[20] W. J. Kong, Y. R. Ji, X. Zhang, H. Wu, Q. T. Zhang, Z. H. Yuan, C. H. Wan, X. F. Han, T. Yu, K. Fukuda, H. Naganuma, and M.-J. Tung, Appl. Phys. Lett. **109**, 132402 (2016).
[21] Y.-W. Oh, S. heon Chris Baek, Y. M. Kim, H. Y. Lee, K.-D. Lee, C.-G. Yang, E.-S. Park, K.-S. Lee, K.-W. Kim, G. Go, J.-R. Jeong, B.-C. Min, H.-W. Lee, K.-J. Lee, and B.-G. Park, Nat. Nanotechnol. **11**, 878 (2016).
[22] N. Perez, E. Martinez, L. Torres, S.-H. Woo, S. Emori, and G. S. D. Beach, Appl. Phys. Lett. **104**, 092403 (2014).
[23] R. Ramaswamy, X. Qiu, T. Dutta, S. D. Pollard, and H. Yang, Appl. Phys. Lett. **108**, 202406 (2016).
[24] J. Yu, X. Qiu, W. Legrand, and H. Yang, Appl. Phys. Lett. **109**, 042403 (2016).
[25] T. Taniguchi, S. Mitani, and M. Hayashi, Phys. Rev. B **92**, 024428 (2015).
[26] M. H. Read and C. Altman, Appl. Phys. Lett. **7**, 51 (1965).
[27] L. A. Clevenger, A. Mutscheller, J. M. E. Harper, C. Cabral, and K. Barmak, J. Appl. Phys. **72**, 4918 (1992).
[28] U. H. Pi, K. W. Kim, J. Y. Bae, S. C. Lee, Y. J. Cho, K. S. Kim, and S. Seo, Appl. Phys. Lett. **97**, 162507 (2010).
[29] J. Kim, J. Sinha, M. Hayashi, M. Yamanouchi, S. Fukami, T. Suzuki, S. Mitani, and H. Ohno, Nat. Mater. **12**, 240 (2012).
[30] M. Hayashi, J. Kim, M. Yamanouchi, and H. Ohno, Phys. Rev. B **89**, 144425 (2014).
[31] H. Wu, C. H. Wan, Z. H. Yuan, X. Zhang, J. Jiang, Q. T. Zhang, Z. C. Wen, and X. F. Han, Phys. Rev. B **92**, 054404 (2015).
[32] X. Fan, H. Celik, J. Wu, C. Ni, K.-J. Lee, V. O. Lorenz, and J. Q. Xiao, Nat. Commun. **5**, 3042 (2014).
[33] H. B. Michaelson, J. Appl. Phys. **48**, 4729 (1977).
[34] H. L. Skriver and N. M. Rosengaard, Phys. Rev. B **46**, 7157 (1992).
[35] S. E. Barnes, J. Ieda, and S. Maekawa, Sci. Rep. **4**, 4105 (2014).
[36] S. Yan and Y. B. Bazaliy, Phys. Rev. B **91**, 214424 (2015).
[37] G. Yu, P. Upadhyaya, K. L. Wong, W. Jiang, J. G. Alzate, J. Tang, P. K. Amiri, and K. L. Wang, Phys. Rev. B **89**, 104421 (2014).
[38] C.-F. Pai, M. Mann, A. J. Tan, and G. S. D. Beach, Phys. Rev. B **93**, 144409 (2016).
[39] J.-C. Rojas-Sánchez, P. Laczkowski, J. Sampaio, S. Collin, K. Bouzehouane, N. Reyren, H. Jaffrès, A. Mougin, and J.-M. George, Appl. Phys. Lett. **108**, 082406 (2016).
[40] A detailed picture is schematically depicted in Fig. 1 of Ref. [38].
[41] K.-S. Lee, S.-W. Lee, B.-C. Min, and K.-J. Lee, Appl. Phys. Lett. **102**, 112410 (2013).